

Spectral representations of the electron energy loss in composite media

Ronald Fuchs

Ames Laboratory and Department of Physics and Astronomy, Iowa State University, Ames, Iowa 50011

Rubén G. Barrera

Instituto de Física, Universidad Nacional Autónoma de México, Apartado Postal 20-364, 01000 México, Distrito Federal, México

José Luis Carrillo

Instituto de Física "Luis Rivera Terrazas," Universidad Autónoma de Puebla, Apartado Postal J-48, 72570 Puebla, Puebla, México

(Received 24 May 1996)

Using a recently developed theory for the inverse longitudinal nonlocal dielectric response for a granular composite [R. G. Barrera and R. Fuchs, *Phys. Rev. B* **52**, 3256 (1995)], we find an effective local dielectric response from the condition that it must give the same electron energy-loss probability density as the actual nonlocal response. This local response is expressed as a spectral representation: a sum of terms with simple poles corresponding to the excitation of bulk and interfacial modes. Taking as a guideline the condition that the strength and location of the poles must satisfy sum rules, a single-surface-mode approximation is proposed. This single-mode approximation is tested for a random system of aluminum spheres in vacuum. [S0163-1829(96)07142-1]

I. INTRODUCTION

In the study of the optical properties of composite materials the concept of an effective medium has been a useful tool for the interpretation of a wide variety of experimental results as well as for a better understanding of the physics of inhomogeneous systems.¹ An effective medium is a fictitious homogeneous medium with the same optical properties as those of the actual composite material. In the case of non-magnetic systems, the linear optical properties are determined by the transverse dielectric function, which relates the transverse components of the displacement and electric fields. Due to the geometrical structure of a composite material, the induced electric fields are highly inhomogeneous at length scales of the order of the spatial inhomogeneities of the system. When one is interested in the average of these fields rather than their spatial fluctuations, the concept of an effective response (or an effective medium) becomes appropriate and useful. An effective (or macroscopic) dielectric response is then defined as the linear operator which relates the *averages* of the displacement and electric fields. The theoretical problem then consists in devising a theory which yields the effective response of a composite material in terms of the response of its constituents and the statistical properties of its geometrical structure. The study of this effective response, for the description of the optical and electrical properties of two-component composites, has a long history which goes back to the end of last century.¹ There are two classic papers, one by Maxwell Garnett² and another by Bruggeman,³ in which simple expressions for the effective dielectric response are derived. These expressions have been widely used for the interpretation of optical data and they have also stimulated the development of more sophisticated and accurate theories⁴.

On the other hand, the application of effective medium

theories to the problem of electron energy loss in composite materials is rather recent. In the works of Walsh⁵ and Howie and Walsh⁶ one finds some of the first attempts to use the concept of an effective medium to construct a theory for the calculation of the electron energy loss in a granular composite. They tried to apply the theories which were successful in the field of optics to the interpretation of their own energy-loss experiments. Lack of success in this task led them to the construction of a phenomenological theory for the calculation of the inverse dielectric response, which is the quantity that governs the electron energy-loss phenomenon. Stimulated by this work, Pendry and Moreno⁷ calculated the energy loss of electrons passing above an ordered array of spheres. Later, Barrera and Fuchs⁸ introduced the effects of disorder by developing a theory for the calculation of the effective inverse dielectric longitudinal response for a random system of spherical inclusions. They showed that taking account of the spatial nonlocality in the response was essential for understanding the energy-loss mechanism. Using this theory, our main objective in this paper is to construct a spectral representation of an effective *local* inverse dielectric response which can be related more directly to the structure of the electron energy-loss spectra. We also propose an approximation for this local response which could be very useful for the actual interpretation of experimental data. The paper has the following structure: In Sec. II we derive a spectral representation for the effective inverse nonlocal dielectric response, together with associated sum rules. The electron energy-loss probability is then calculated and the effective local inverse dielectric response is defined and written in a spectral form. In Sec. III we introduce and analyze the multiple- and single-surface-mode approximations for the local response. In the last part of this section the accuracy of the single-surface-mode approximation is tested for a model of random spheres in vacuum. Section IV is devoted

to comparing our single-surface-mode approximation with the phenomenological theory developed by Howie and Walsh,⁶ and Sec. V is a summary of the paper.

II. SPECTRAL REPRESENTATIONS OF THE DIELECTRIC RESPONSE

A. Inverse longitudinal dielectric function

Consider an external electric potential with wave vector \mathbf{k} and frequency ω exciting a homogeneous and isotropic system. According to linear response theory, the Fourier transform of the induced potential will be given by

$$V^{\text{ind}}(\mathbf{k}, \omega) = [\varepsilon^{-1}(\mathbf{k}, \omega) - 1] V^{\text{ext}}(\mathbf{k}, \omega), \quad (1)$$

where $V^{\text{ind}}(k, \omega)$ and $V^{\text{ext}}(\mathbf{k}, \omega)$ are the (\mathbf{k}, ω) Fourier components of the induced and external potentials, respectively, and $\varepsilon^{-1}(\mathbf{k}, \omega)$ is the corresponding Fourier component of what is known as the inverse longitudinal dielectric response of the system. Here ε^{-1} depends only on $k = |\mathbf{k}|$, due to the isotropy of the system.

For an inhomogeneous system, a given \mathbf{k} th Fourier component of the external field will, in general, excite an induced potential with Fourier components $\mathbf{k}' \neq \mathbf{k}$; thus its inverse dielectric response will be given by $\varepsilon^{-1}(\mathbf{k}, \mathbf{k}'; \omega)$. Here we will consider granular systems which are inhomogeneous on a certain length scale but appear homogeneous on a larger length scale, which will be called macroscopic. Our purpose here is to calculate an effective or macroscopic inverse dielectric response which appears in a linear relation between the external field and the average induced field, when this average is performed over the macroscopic length scale. It can be shown that under a translational average the only Fourier components that survive in $\varepsilon^{-1}(\mathbf{k}, \mathbf{k}'; \omega)$ are those with $\mathbf{k}' = \mathbf{k}$. If we further assume that the system appears to be isotropic after the performance of a configurational average, the effective or macroscopic longitudinal inverse dielectric response $\varepsilon_M^{-1}(k, \omega)$ is then defined by

$$\langle V^{\text{ind}}(\mathbf{k}, \omega) \rangle = [\varepsilon_M^{-1}(k, \omega) - 1] V^{\text{ext}}(\mathbf{k}, \omega), \quad (2)$$

where $\langle \dots \rangle$ means configurational average.

A breakthrough in the study of the effective dielectric response of composite materials was the introduction of its spectral representation. It was shown^{9,10} that in the $k \rightarrow 0$ limit the macroscopic dielectric response $\varepsilon_M(\omega) \equiv \varepsilon_M(k \rightarrow 0, \omega)$ of any macroscopically homogeneous and isotropic two-component system can be expressed as a sum (or integral) of simple poles, that is,

$$\varepsilon_M(\omega) = \varepsilon_2(\omega) \left[1 - f \sum_v \frac{C_v}{u - n_v} \right], \quad (3)$$

where

$$u = \frac{-1}{\varepsilon_1(\omega)/\varepsilon_2(\omega) - 1} \quad (4)$$

is the spectral variable, $\varepsilon_1(\omega)$ and $\varepsilon_2(\omega)$ are the local dielectric functions of each of the two components, and f is the filling fraction of component 1. This is actually a representation in normal modes: The position of the poles $u = n_v$ corresponds to the resonant frequencies of the normal modes

of the electric field in the system and the C_v correspond to their strengths. The n_v are called the depolarization factors.

It has been recently shown⁸ that for a system made of spherical inclusions distributed at random within an otherwise homogeneous matrix, a spectral representation for the macroscopic inverse longitudinal dielectric response $\varepsilon_M^{-1}(k, \omega)$ also exists. This spectral representation has the form

$$\varepsilon_M^{-1}(k, \omega) = \frac{1}{\varepsilon_2} \left[1 + f \left(\frac{C_b}{u-1} + \sum_s \frac{C_s}{u-n_s} \right) \right], \quad (5)$$

where u is the same spectral variable defined in Eq. (4), and $\varepsilon_1(\omega)$ and $\varepsilon_2(\omega)$ are the local dielectric responses of the spheres and matrix, respectively.¹¹ Here and below we omit the explicit dependence on k and ω in expressions like the right-hand side (RHS) of Eq. (5) to simplify the notation. It should be noted that the spectral representation of $\varepsilon_M^{-1}(k, \omega)$ is very similar to the one given for $\varepsilon_M(k \rightarrow 0, \omega)$ in Eq. (3). Here $u = 1$ ($\varepsilon_1 = 0$) corresponds to the position of the bulk mode of the inclusions and $u = n_s$ corresponds to the position of the interfacial modes. In the bulk modes the induced charge density is located in the interior of the spheres, while in the interfacial modes it is located at their surfaces. Consequently, C_b is the strength of the bulk mode of the spheres and the C_s are the strengths of the interfacial modes. The strength and positions of the modes depend on the wave vector k of the external field, the radius a of the spheres, their filling fraction f , and their geometrical arrangement. It can be shown⁸ that

$$C_b + \sum_s C_s = 1, \quad (6)$$

which states that the sum of the strengths of all modes is conserved.

In the mean-field approximation the statistical properties of the geometrical arrangement of the spheres are determined completely by their filling fraction f and their two-particle distribution function $\rho^{(2)}(R_{12})$. Here $R_{12} \equiv |\mathbf{R}_1 - \mathbf{R}_2|$ is the distance between a pair of spheres whose centers are located at \mathbf{R}_1 and \mathbf{R}_2 , respectively. If one takes account only of the correlations coming from the excluded volume of the spheres, that is,

$$\rho^{(2)}(R_{12}) = \begin{cases} 0 & \text{if } R_{12} < 2a, \\ 1 & \text{if } R_{12} \geq 2a, \end{cases} \quad (7)$$

one gets simple expressions for the strengths and positions of the modes which are given explicitly in Appendix A.

In the spectral representation given by Eq. (5), the mode corresponding to the bulk mode of the matrix ($\varepsilon_2 = 0$) has not been isolated: i.e., the factor $1/\varepsilon_2$ does not appear in a separate term, but multiplies the whole expression in square brackets. One is able to isolate the bulk mode of the matrix by rewriting Eq. (5) in a more symmetric form

$$\varepsilon_M^{-1}(k, \omega) = \sum_j \frac{G_j}{n_j \varepsilon_1 + (1 - n_j) \varepsilon_2}, \quad (8)$$

where j runs over all modes: the bulk mode of the matrix b_1 with $n_{b_1} = 1$, the bulk mode of the spheres b_2 with

$n_{b_2}=0$, and the interfacial modes s with n_s ($0 \leq n_s \leq 1$) given by Eq. (A4). The corresponding strengths G_j of the modes are given by

$$G_{b_1} = f C_b, \quad (9)$$

$$G_{b_2} = 1 - f - f \sum_s \left(\frac{1}{n_s} - 1 \right) C_s, \quad (10)$$

and

$$G_s = f \frac{C_s}{n_s}. \quad (11)$$

Here G_{b_1} and G_{b_2} are the strengths of the bulk modes of media 1 and 2, respectively, and the G_s are the strengths of the interfacial modes when both materials are considered to be *active*. These relations between the G_j and $\{f, C_b, C_s, n_s\}$ are valid in general; this means that they would be also valid in an exact theory. Using Eq. (6) one can show that these strengths G_j obey the sum rules

$$\sum_j G_j = 1, \quad (12)$$

$$\sum_j n_j G_j = f_1, \quad (13)$$

and combining these two one can write

$$\sum_j (1 - n_j) G_j = f_2, \quad (14)$$

where $f_1 \equiv f$ is the filling fraction of medium 1 and $f_2 \equiv 1 - f$ is the corresponding filling fraction of medium 2. The resonant frequencies are determined by the vanishing of the denominators in Eq. (8).

B. Electron energy-loss probability density

We now use the spectral representation given in Eq. (8) to derive a corresponding representation for the electron energy-loss probability density $\Xi(E)$ of a beam of fast electrons traveling through the system. The electrons have an incident energy E_I and lose energy by exciting collective modes of energy $E = \hbar \omega$. Here $\Xi(E)$ is defined as in Ref. 8,

$$\Xi(E) = a_0 E_I \frac{d^2 P(E)}{d l d E}, \quad (15)$$

where a_0 is the Bohr radius and $d^2 P(E)/d l d E$ is the probability per unit length, per unit energy, for an electron to scatter with energy loss E . The relation between $\Xi(E)$ and $\varepsilon_M^{-1}(k, \omega)$ is given by⁸

$$\Xi(E) = \frac{1}{\pi} \int_{\omega/v_I}^{k_c} \text{Im}[-\varepsilon_M^{-1}(k, \omega)] \frac{d k}{k}, \quad (16)$$

where v_I is the speed of the incident electrons, and k_c is an upper cutoff wave vector usually determined by the angular aperture of the electron energy-loss detector.

We now define an effective *local* dielectric response $\varepsilon_{\text{eff}}(\omega)$ through the expression

$$\frac{1}{\varepsilon_{\text{eff}}(\omega)} = W \int_{\omega/v_I}^{k_c} \varepsilon_M^{-1}(k, \omega) \frac{d k}{k}, \quad (17)$$

where $1/W = \ln k_c v_I / \omega$. Using these definitions one is now able to write

$$\pi \Xi(E) = \frac{1}{W} \text{Im} \left[\frac{-1}{\varepsilon_{\text{eff}}(\omega)} \right], \quad (18)$$

which looks formally identical to the corresponding expression for the electron energy-loss probability density through a homogeneous medium with dielectric response $\varepsilon_{\text{eff}}(\omega)$.

Now, inserting Eq. (8) into Eq. (17) and writing the bulk mode terms $j=b_1, b_2$ separately from the interfacial mode terms $j=s$, one finds

$$\frac{1}{\varepsilon_{\text{eff}}} = \frac{A_{b_1}}{\varepsilon_1} + \frac{A_{b_2}}{\varepsilon_2} + W \int_{\omega/v_I}^{k_c} \sum_s \frac{G_s}{n_s \varepsilon_1 + (1 - n_s) \varepsilon_2} \frac{d k}{k}, \quad (19)$$

where

$$A_j = W \int_{\omega/v_I}^{k_c} G_j(k) \frac{d k}{k} \quad (20)$$

for $j=b_1$ and b_2 . To simplify the notation we have omitted both the dependence of $G_s(k)$ and $n_s(k)$ on k in the third term on the right-hand side of Eq. (19) and the explicit dependence of ε_1 , ε_2 , and ε_{eff} on ω .

In this equation $1/\varepsilon_{\text{eff}}$ is given as a sum of two discrete poles at $\varepsilon_1=0$ and $\varepsilon_2=0$, corresponding to the bulk modes, plus an integral over k of a sum of terms containing simple poles at $n_s(k) \varepsilon_1 + [1 - n_s(k)] \varepsilon_2 = 0$, corresponding to the interfacial modes. A_{b_1} and A_{b_2} are the effective strengths of the *bulk* energy loss in media 1 and 2, respectively. In a strict sense, one cannot call Eq. (19) a spectral representation of $1/\varepsilon_{\text{eff}}$, because the third term in the right-hand side is not expressed as an integral over the depolarization factors, as required in the original definition of the spectral representation.⁹ Nevertheless, Eq. (19) can be put in the canonical form of a spectral representation by an appropriate change of integration variable in the integrals over k . First consider k a (multivalued) function of n_s , $k=k(n_s)$, and then move the function labels from n to k , so that $k=k(n_s)$ can be rewritten as $k_s=k_s(n)$. Then the variable of integration can be changed from k_s to n , yielding

$$W \int_{\omega/v_I}^{k_c} \frac{G_s}{n_s \varepsilon_1 + (1 - n_s) \varepsilon_2} \frac{d k}{k} = W \int_0^1 \frac{G_s[k_s(n)]}{n \varepsilon_1 + (1 - n) \varepsilon_2} \left| \frac{d k_s}{d n} \right| \frac{d n}{k_s(n)} \quad (21)$$

$$= \int_0^1 \frac{\mathcal{A}_s(n)}{n \varepsilon_1 + (1 - n) \varepsilon_2} d n, \quad (22)$$

where

$$\mathcal{A}_s(n) = W G_s[k_s(n)] \left| \frac{d k_s}{d n} \right| \frac{1}{k_s(n)} \quad (23)$$

is the continuous spectral function associated with the interfacial mode s . Now, substituting Eq. (22) into Eq. (19), we obtain the spectral representation of $1/\varepsilon_{\text{eff}}$ in canonical form, that is,

$$\frac{1}{\varepsilon_{\text{eff}}} = \frac{A_{b_1}}{\varepsilon_1} + \frac{A_{b_2}}{\varepsilon_2} + \int_0^1 \frac{\mathcal{A}(n)}{n\varepsilon_1 + (1-n)\varepsilon_2} dn, \quad (24)$$

where

$$\mathcal{A}(n) = \sum_s \mathcal{A}_s(n) \quad (25)$$

is the spectral function associated with the continuous distribution of all interfacial modes.

An actual calculation of the integrals over the depolarization factors given in Eqs. (21), (22), and (24) would require one to take into account the fact that k_s is, in general, a multiple-valued function of n . This means that the integration over n should be performed over each branch of the function $k_s(n)$ that lies within the range of integration $\omega/v_1 \leq k_s \leq k_c$. To avoid cumbersome notation we have omitted a sum over branches and used the values 0 and 1 as limits in the integration over n instead of specifying the actual limits for each branch, which always lie between 0 and 1. This simplified notation is justified since the spectral functions $\mathcal{A}_s(n)$ have been introduced as conceptual tools; Eqs. (20)–(25) are never actually used to compute $1/\varepsilon_{\text{eff}}$.

As a result of the k integration in Eq. (17), the strengths A_{b_1} and A_{b_2} , as well as the $\mathcal{A}_s(n)$, now depend on $\{\omega, k_c, v_1\}$, in contrast with the spectral representation of $\varepsilon_M^{-1}(k, \omega)$, given in Eq. (8), where the strengths of the poles depend only on structural parameters. Also, while the bulk modes appear as isolated poles in the complex ω plane, the interfacial modes correspond to a continuous branch cut.

It is not difficult to show that as a consequence of Eqs. (12) and (13) the following sum rules are always fulfilled:

$$A_{b_1} + A_{b_2} + \int_0^1 \mathcal{A}(n) dn = 1 \quad (26)$$

and

$$A_{b_1} + \int_0^1 n \mathcal{A}(n) dn = f_1. \quad (27)$$

The total strength of bulk and interfacial modes is always conserved and adds to one, as stated in Eq. (26), while the second sum rule, Eq. (27), determines the centroid of the mode distribution. The main merit of the spectral representation given by Eq. (24) is its direct relationship with the experimental energy-loss spectra through Eq. (18).

Structural information about the system can be obtained, for example, by analyzing how the strengths and positions of the modes depend on f , a , and ω , for a given incident energy E_I and wave vector cutoff k_c . The simplest case for studying this dependence is to consider the strengths of the bulk modes. Each bulk mode generally occurs at a single frequency, and so the bulk modes are usually identified as well-defined peaks in the energy-loss spectra. The strength of the bulk modes is proportional to the height of these peaks, and their width is due to the presence of different kinds of

dissipation mechanisms within the system. The corresponding analysis for the interfacial modes is more complex, not only because of the more intricate dependence of $\mathcal{A}(n)$ on the structural parameters of the system, but also because $\mathcal{A}(n)$ depends on the frequency ω . Nevertheless, this analysis can be greatly simplified whenever the single-pole approximation, developed in the next section, can be used.

The dependence of A_{b_1} and A_{b_2} on f , a , and ω can be studied by substituting Eqs. (9) and (10) into Eq. (20). One gets

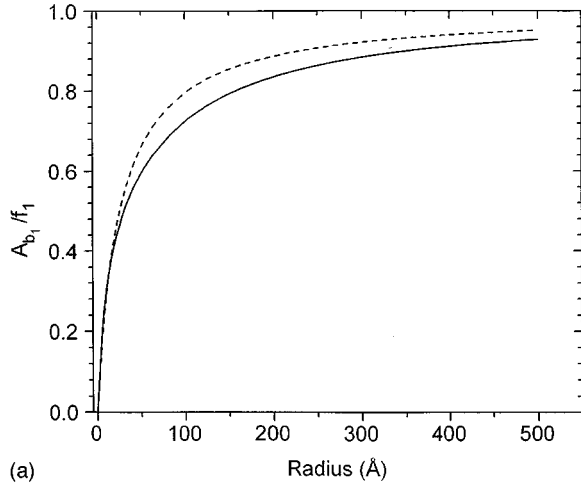
$$A_{b_1} = W f_1 \int_{\omega a/v_1}^{k_c a} C_b(x) \frac{dx}{x} \quad (28)$$

and

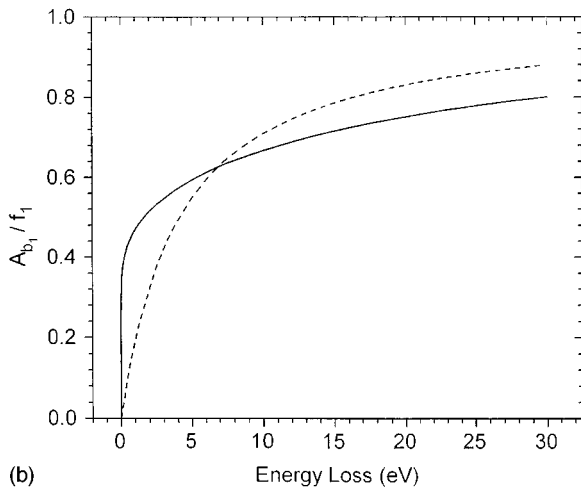
$$A_{b_2} = 1 - f_1 - W f_1 \sum_s \int_{\omega a/v_1}^{k_c a} \left(\frac{1}{n_s(x)} - 1 \right) C_s(x) \frac{dx}{x}, \quad (29)$$

which can be evaluated using the expressions for $C_b(ka)$, $n_s(ka)$, and $C_s(ka)$ given by Eqs. (A1), (A2) and (A4) in Appendix A. One can see that A_{b_1} is proportional to f_1 and is given in terms of a well-behaved integral, because $C_b(ka)$ goes as $(ka)^2$ for small ka and approaches 1 asymptotically for large ka . For ω finite, one can show from Eq. (28) that $A_{b_1} \rightarrow 0$ in the limit $a \rightarrow 0$ and $A_{b_1} \rightarrow f_1$ when $a \rightarrow \infty$; thus $0 \leq A_{b_1}/f_1 \leq 1$, for $0 \leq a \leq \infty$. The direct proportionality of A_{b_1} with f_1 also means that A_{b_1}/f_1 represents the strength of the bulk energy loss for an *isolated* sphere. Thus the deviation of A_{b_1}/f_1 from 1 is a manifestation of the *Begrenzung* effect in an isolated sphere. The fact that all spheres are identical (and therefore have the same *Begrenzung* effect) is what makes A_{b_1} directly proportional to f_1 . The solid line in Fig. 1(a) shows A_{b_1}/f_1 as a function of the radius a of the spheres measured in Å, for $k_c = 1.69 \text{ \AA}^{-1}$, electrons with incident energy $E_I = 100 \text{ keV}$ and energy loss $\hbar\omega = 16 \text{ eV}$ which corresponds to the plasmon energy $\hbar\omega_p$ [$\varepsilon_1(\omega_p) = 0$] in aluminum. We can see how the strength increases with the particle size and how it tends asymptotically to 1 as a increases. The solid line in Fig. 1(b) shows A_{b_1}/f_1 as a function of the energy loss $\hbar\omega$ measured in eV, for a fixed sphere radius $a = 100 \text{ \AA}$ and for $k_c = 1.69 \text{ \AA}^{-1}$ and $E_I = 100 \text{ keV}$. The external parameters $E_I = 100 \text{ keV}$ and $k_c = 1.69 \text{ \AA}^{-1}$ are typical in a standard scanning transmission electron microscope with an aperture 0.01 rad in the electron detection.

The effective strength of the bulk energy loss in medium 2 is A_{b_2} . This medium is connected and has a complicated geometry; it fills the complementary space left by the spherical inclusions. For ω finite, one can show from Eq. (29) that $A_{b_2} \rightarrow (1 - f_1)/(1 + 2f_1)$ in the limit $a \rightarrow 0$ and $A_{b_2} \rightarrow 1 - f_1$ when $a \rightarrow \infty$; thus $1/(1 + 2f_1) \leq A_{b_2}/f_2 \leq 1$, for $0 \leq a \leq \infty$. Therefore, for finite a , A_{b_2} does not scale with f_2 , as shown in Fig. 2, complicating the direct determination of the structural parameters from experiment. In Fig. 2(a) we plot A_{b_2}/f_2 as a function of the radius a of the spheres for $k_c = 1.69 \text{ \AA}^{-1}$, $E_I = 100 \text{ keV}$, $\hbar\omega = 16 \text{ eV}$, and $f_1 = 0.1$ and



(a)

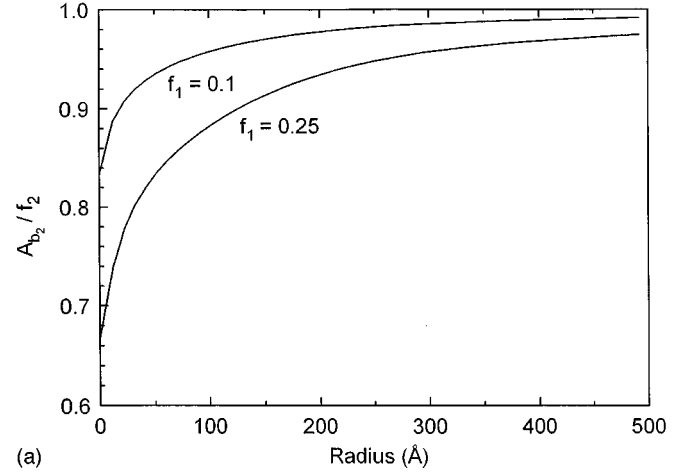


(b)

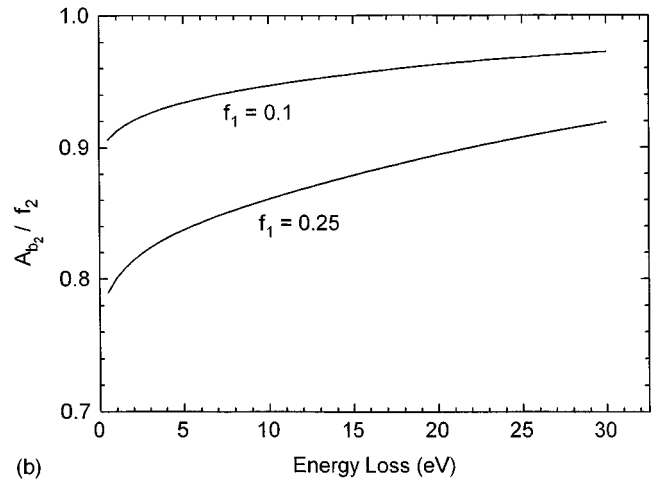
FIG. 1. (a) Strength of the bulk mode A_{b_1} over the filling fraction f_1 as a function of the radius a (in \AA) of the spheres, for an energy loss $\hbar\omega = 16$ eV, upper wave vector cutoff $k_c = 1.69 \text{ \AA}^{-1}$, and incident energy $E_I = 100$ keV. The dashed line is the corresponding expression $A_{b_1}^{\text{HW}}/f_1$ proposed by Howie and Walsh as discussed in the text. (b) Strength of the bulk mode A_{b_1} over the filling fraction f_1 as a function of the energy loss $\hbar\omega$ (in eV), for spheres of radius $a = 100 \text{ \AA}$, upper wave vector cutoff $k_c = 1.69 \text{ \AA}^{-1}$, and incident energy $E_I = 100$ keV. The dashed line is the corresponding expression $A_{b_1}^{\text{HW}}/f_1$ proposed by Howie and Walsh as discussed in the text.

0.25. In Fig. 2(b) we plot A_{b_2}/f_2 as a function of the energy loss $\hbar\omega$ for $k_c = 1.69 \text{ \AA}^{-1}$, $E_I = 100$ keV, $a = 100 \text{ \AA}$, and $f_1 = 0.1$ and 0.25. In these figures one can see that for a given filling fraction f_1 , A_{b_2}/f_2 increases as either the radius of the spheres or the energy loss increase. Also, for a given radius or energy loss, A_{b_2}/f_2 decreases as f_1 increases.

In conclusion, for an electron beam of a given energy, the measurement of the relative height of the energy-loss peaks corresponding to the strength of the bulk modes does not determine f and a separately. A precise determination of these quantities requires a detailed analysis of the energy-loss spectra corresponding to the interfacial modes, as has been already shown in Ref. 8, for the case of aluminum spheres in AlF_3 .



(a)



(b)

FIG. 2. (a) Strength of the bulk mode A_{b_2} over the filling fraction f_2 as a function of the radius a (in \AA) of the spheres, for an energy loss $\hbar\omega = 16$ eV, upper wave vector cutoff $k_c = 1.69 \text{ \AA}^{-1}$, incident energy $E_I = 100$ keV, and filling fractions $f_1 = 0.1$ and 0.25. (b) Strength of the bulk mode A_{b_2} over the filling fraction f_2 as a function of the energy loss $\hbar\omega$ (in eV), for spheres of radius $a = 100 \text{ \AA}$, upper wave vector cutoff $k_c = 1.69 \text{ \AA}^{-1}$, incident energy $E_I = 100$ keV, and filling fractions $f_1 = 0.1$ and 0.25.

III. DISCRETE SURFACE-MODE APPROXIMATION

A. Multiple-surface-mode approximation

In the multiple-surface-mode approximation the idea is to replace the continuous spectrum of the interfacial modes which appears in Eq. (24) by an infinite sum of simple poles. The weights A_s and the locations α_s of these poles are chosen so as to fulfill the same sum rules as the ones fulfilled by the continuous spectrum, that is,

$$A_{b_1} + A_{b_2} + \sum_s A_s = 1 \quad (30)$$

and

$$A_{b_1} + \sum_s \alpha_s A_s = f_1, \quad (31)$$

which are the discrete counterparts of Eqs. (26) and (27). This leads immediately to the following definitions of A_s and α_s ,

$$A_s = \int_0^1 \mathcal{A}_s(n) dn \quad (32)$$

and

$$\alpha_s A_s = \int_0^1 n \mathcal{A}_s(n) dn. \quad (33)$$

Therefore $\varepsilon_{\text{eff}}(\omega)$ can be written as

$$\frac{1}{\varepsilon_{\text{eff}}} \approx \frac{A_{b_1}}{\varepsilon_1} + \frac{A_{b_2}}{\varepsilon_2} + \sum_s \frac{A_s}{\alpha_s \varepsilon_1 + (1 - \alpha_s) \varepsilon_2}. \quad (34)$$

Explicit expressions for A_s and α_s are derived in Appendix B. Equation (34) is the best possible discrete approximation to the actual spectral representation [Eq. (24)] in the sense that each discrete interfacial mode has the same strength A_s and position α_s as the total strength and centroid of the corresponding continuous mode. The strength and location of these discrete poles can be easily determined in the dilute ($f_1 \rightarrow 0$) limit, which corresponds to the case of non-interacting spheres. In this case, one gets

$$A_s = f_1 3(2s+1)^2 W \int_{\omega a/v_1}^{k_c a} \frac{j_s^2(x)}{x^3} dx \quad (35)$$

and

$$\alpha_s = \frac{s}{2s+1}, \quad (36)$$

where s labels the multipolar order of the induced interface modes on the noninteracting spheres. Thus $s=1$ corresponds to the dipolar mode, $s=2$ to the quadrupolar mode, etc. To lowest order in f_1 , while the strengths A_s of the interfacial modes are proportional to f_1 , their positions $\alpha_s = 1/3, 2/5, 3/7, \dots$, are independent of f_1 and lie within the interval $1/3 \leq \alpha_s \leq 1/2$, the value $1/2$ being an accumulation point. In Figs. 3(a) and 3(b) we plot, for the first three modes, A_s/f_1 as a function of a and $\hbar\omega$, respectively, for $k_c = 1.69 \text{ \AA}^{-1}$ and $E_I = 100 \text{ keV}$. In Fig. 3(a), $\hbar\omega = 16 \text{ eV}$, and in Fig. 3(b) $a = 100 \text{ \AA}$. These figures show that, with these selections of parameters, the dipolar mode dominates over higher multipolar modes only in the region of small radii and small energy losses. Its strength decays rapidly with increasing energy loss or radius. For example, for $\hbar\omega = 16 \text{ eV}$ and $a \approx 30 \text{ \AA}$, or $a = 100 \text{ \AA}$ and $\hbar\omega \approx 5 \text{ eV}$, the strength of the sum of the quadrupolar and octupolar modes is already about half of the strength of the dipolar mode. Finally, recall that to lowest order in f_1 , A_s/f_1 are the corresponding mode strengths for an isolated sphere.

B. Single-surface-mode approximation

As f_1 increases, the dependence of the strengths A_s and locations α_s of the interfacial modes on f_1 becomes more complicated and the whole analysis of extracting structural information from $1/\varepsilon_{\text{eff}}$ becomes more involved. Nevertheless, a simple situation arises when the resonant energies of

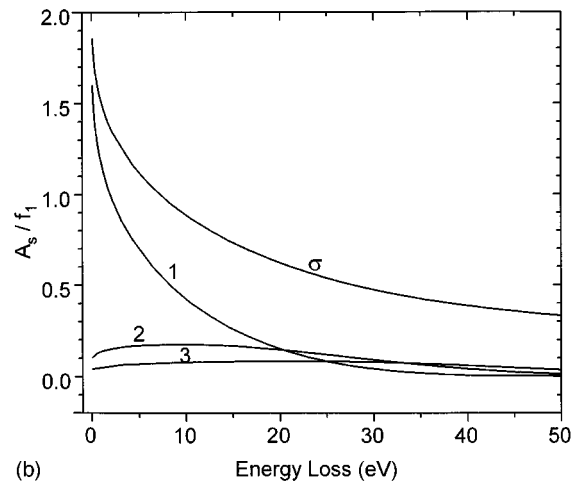
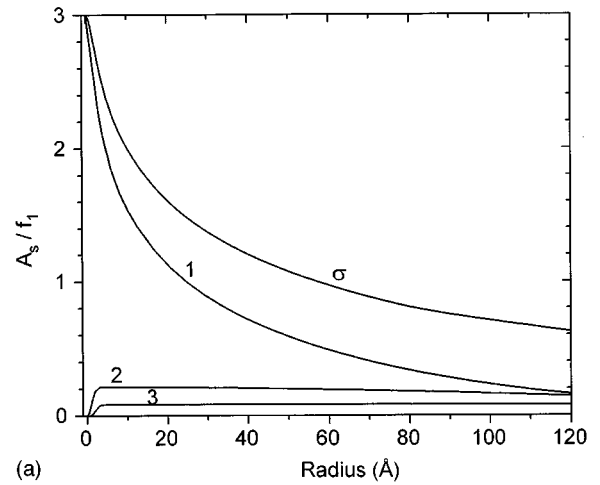


FIG. 3. (a) Strength of the interfacial modes A_s over the filling fraction f_1 as a function of the radius a (in \AA) of the spheres, in the low-density limit ($f_1 \rightarrow 0$), for an energy loss $\hbar\omega = 16 \text{ eV}$, upper wave vector cutoff $k_c = 1.69 \text{ \AA}^{-1}$, and incident energy $E_I = 100 \text{ keV}$. The numbers 1,2,3 above each line label the first three modes $s=1,2,3$ and the letter σ labels the effective single mode $s=\sigma$. (b) Strength of the interfacial modes A_s over the filling fraction f_1 as a function of the energy loss $\hbar\omega$ (in eV), in the low-density limit ($f_1 \rightarrow 0$), for spheres of radius $a = 100 \text{ \AA}$, upper wave vector cutoff $k_c = 1.69 \text{ \AA}^{-1}$, and incident energy $E_I = 100 \text{ keV}$. The numbers 1,2,3 above each line label the first three modes $s=1,2,3$ and the letter σ labels the effective single modes $s=\sigma$.

the interfacial modes lie so close together and the dissipation broadening contained in the imaginary parts of ε_1 and ε_2 is so large that they appear as a single peak in the energy-loss spectrum. In this case it is possible to approximate the infinite set of interfacial modes by a single effective surface mode. The strength and location of this effective surface mode will be labeled A_σ and α_σ , respectively, and they are chosen as to satisfy the sum rules given by Eqs. (30) and (31). This yields

$$A_\sigma = \sum_s A_s \quad (37)$$

and

$$\alpha_\sigma A_\sigma = \sum_s \alpha_s A_s, \quad (38)$$

and the approximation will be called the single-surface-mode approximation. In this approximation $\varepsilon_{\text{eff}}(\omega)$ is simply written as,

$$\frac{1}{\varepsilon_{\text{eff}}} \approx \frac{A_{b_1}}{\varepsilon_1} + \frac{A_{b_2}}{\varepsilon_2} + \frac{A_\sigma}{\alpha_\sigma \varepsilon_1 + (1 - \alpha_\sigma) \varepsilon_2}, \quad (39)$$

and the sum rules become

$$A_{b_1} + A_{b_2} + A_\sigma = 1 \quad (40)$$

and

$$A_{b_1} + \alpha_\sigma A_\sigma = f_1. \quad (41)$$

The expression for $1/\varepsilon_{\text{eff}}$ in this approximation has an extremely simple and appealing form. From the definitions in Eqs. (37) and (38) it follows that the single effective interfacial mode in the spectral representation of Eq. (39) has the same strength A_σ and position α_σ as the total strength and centroid of all interfacial modes in the actual spectral representation [Eq. (24)], i.e., $A_\sigma = \int_0^1 A(n) dn$ and $\alpha_\sigma = \int_0^1 n A(n) dn / \int_0^1 A(n) dn$. Furthermore, it can be seen from Eqs. (40) and (41) that A_σ and α_σ are completely determined by A_{b_1} , A_{b_2} , and f_1 . Nevertheless, for the case of spherical inclusions and within the approximations used in Appendix A, it is more convenient to calculate α_σ first, and then to determine A_σ from α_σ and A_{b_1} using Eq. (41). The reason for this is that for spheres of radius $a \gg 1/k_c$, α_σ becomes independent of k_c , and what is more important, it becomes only a function of $\omega a/v_I$. To see this, one uses Eqs. (37) and (38) together with Eqs. (B6) to write α_σ as

$$\alpha_\sigma = \sum_s \int_{\omega a/v_I}^{k_c a} C_s(x) \frac{dx}{x} \bigg/ \sum_s \int_{\omega a/v_I}^{k_c a} \frac{C_s(x)}{n_s(x)} \frac{dx}{x}, \quad (42)$$

where $C_s(x)$ and $n_s(x)$ are the strengths and depolarization factors of the interfacial modes as functions of ka , given by Eqs. (A3) and (A4), respectively. Since $C_s(x) \rightarrow 0$ quite rapidly as $x \rightarrow \infty$, α_σ will become independent of the upper limit of integration whenever $k_c a \gg 1$. One can check that this will be the case for $k_c a \approx 10$. This condition is not very restrictive; for example, as pointed out before, for 100 keV electrons in a standard transmission scanning electron microscope a typical value of k_c is about 1.7 \AA^{-1} ; this means that $k_c a \approx 10$ is already fulfilled for spheres of radius of about 17 \AA . Therefore, we will consider here the case $k_c a \gg 1$, and analyze α_σ as a function of the lower limit of integration $\omega a/v_I$. This is very convenient for the analysis of experimental data since the dependence on frequency and the external parameters is combined in a single variable.

In Fig. 4 we show the position α_σ of the single effective surface mode as a function of $\omega a/v_I$, for different values of the filling fraction f_1 . In reading this graph one must recall that the values very close to the origin on the $\omega a/v_I$ axis are not very accurate, because the present calculation of α_σ is not valid for $a \rightarrow 0$; it is valid only if $a \gg 1/k_c$. In the limit $a \rightarrow 0$, the only active mode is the dipolar one, and one can show that $\alpha_\sigma(a \rightarrow 0) = (1 + 2f_1)/3$. Therefore, in Fig. 4 we

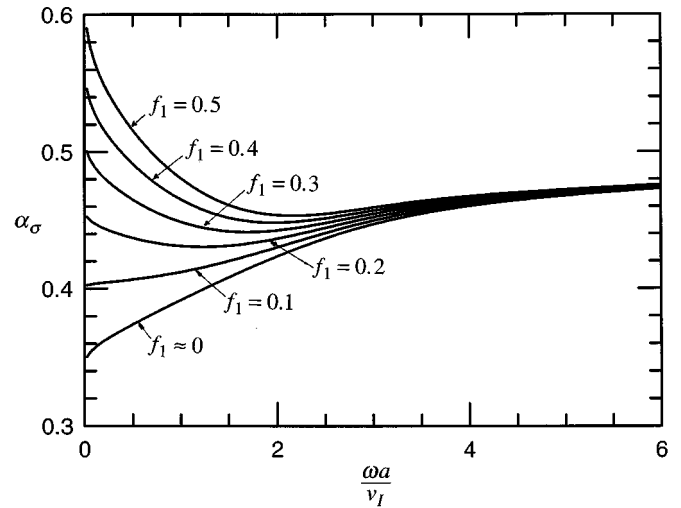


FIG. 4. Position α_σ of the effective single mode as a function of $\omega a/v_I$ for different filling fractions f_1 . The label $f_1 \approx 0$ corresponds to the low density limit ($f_1 \rightarrow 0$).

see that for $\omega a/v_I \approx 0$, α_σ starts around the values $(1 + 2f_1)/3$ for each value of f_1 , and then goes asymptotically to the value $1/2$, for all f_1 , as $\omega a/v_I$ increases. For $f_1 = 0.2$ one sees that α_σ has actually a minimum around $\omega a/v_I \approx 1.3$. The curve labeled $f_1 \approx 0$ corresponds to the dilute ($f_1 \rightarrow 0$) limit which corresponds to the case of an isolated sphere. To get some idea of typical values of the parameter $\omega a/v_I$, note that $\omega a/v_I = 0.924$ when the energy loss $\hbar\omega = 10.0 \text{ eV}$, the sphere radius $a = 100 \text{ \AA}$, and the incident electron energy $E_I = 100 \text{ keV}$. In Appendix C we give a convenient formula [Eq. (C9)] for calculating $\omega a/v_I$ for arbitrary values of $\hbar\omega$, a , and E_I . Finally, we must remark that the way α_σ approaches its limiting value $(1 + 2f_1)/3$ along the $\omega a/v_I$ axis depends on whether one considers $a \rightarrow 0$ or $\omega \rightarrow 0$; when $\omega \rightarrow 0$ the approach is logarithmic whereas when $a \rightarrow 0$ the approach is a power law.

We now proceed to the calculation of the effective strength A_σ by using Eq. (41); that is, $A_\sigma = (f_1 - A_{b_1})/\alpha_\sigma$. Nevertheless, it will be illustrative to first calculate A_σ in the dilute ($f_1 \rightarrow 0$) limit, since in this limit A_σ corresponds to the effective strength for an isolated sphere. This calculation can be performed by using Eq. (37) directly, that is, $A_\sigma = \sum_s A_s$, with the A_s taken from Eq. (35). Since the strengths A_s are proportional to f_1 , the effective strength $A_\sigma = \sum_s A_s$ will be also proportional to f_1 . In Fig. 3 we show the dependence of A_σ/f_1 as a function of the radius of the spheres and the energy loss, for $E_I = 100 \text{ keV}$ and $k_c = 1.69 \text{ \AA}^{-1}$. Here we have performed the sum over all multipolar modes until convergence was attained. Notice again that the contribution of the dipolar mode is dominant only in the region of small radius and small energy loss.

As the filling fraction f_1 increases, A_σ no longer scales with f_1 but it can be calculated, as mentioned above, using Eq. (41). Taking $k_c = 1.69 \text{ \AA}^{-1}$ and $E_I = 100 \text{ keV}$ as external parameters and two filling fractions $f_1 = 0.1$ and 0.25 , in Fig. 5(a) we plot A_σ as a function of a for $\hbar\omega = 16 \text{ eV}$, and in Fig. 5(b) as a function of $\hbar\omega$ for $a = 100 \text{ \AA}$. Since $A_\sigma(a \rightarrow 0) = 3f_1/(1 + 2f_1)$ and $A_\sigma(a \rightarrow \infty) = 0$, the effective

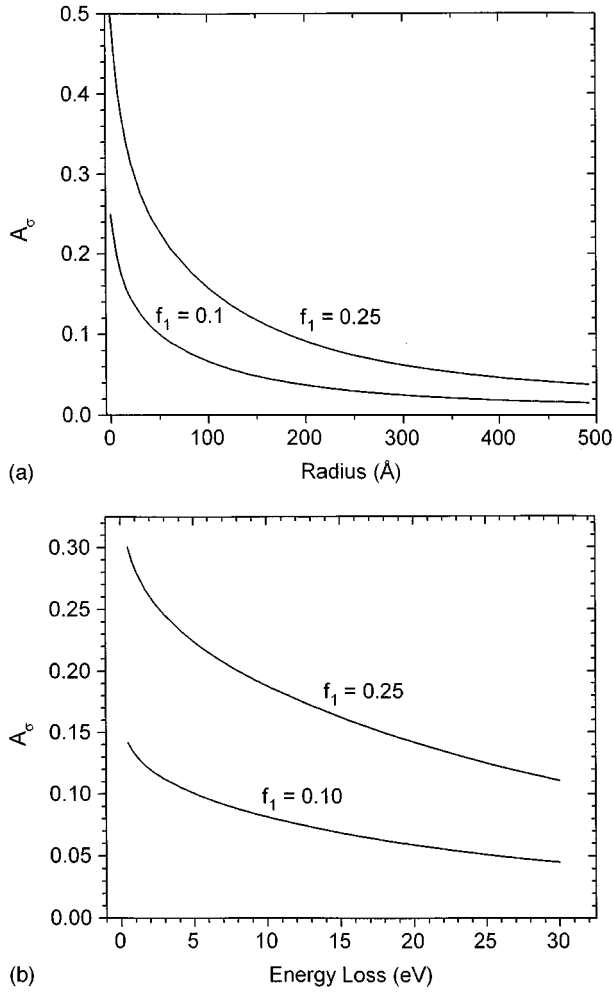


FIG. 5. (a) Strength A_σ of the effective single mode as a function of the radius a (in Å) of the spheres, for an energy loss $\hbar\omega = 16$ eV, upper wave vector cutoff $k_c = 1.69 \text{ \AA}^{-1}$, incident energy $E_I = 100$ keV, and filling fractions $f_1 = 0.1$ and 0.25 . (b) Strength A_σ of the effective single mode as a function of the energy loss $\hbar\omega$ (in eV), for spheres of radius $a = 100$ Å, upper wave vector cutoff $k_c = 1.69 \text{ \AA}^{-1}$, incident energy $E_I = 100$ keV, and filling fractions $f_1 = 0.1$ and 0.25 .

strength A_σ , as a function of a , lies between $0 \leq A_\sigma \leq 3f_1/(1+2f_1)$, and Fig. 5(a) shows that the decrease from $3f_1/(1+2f_1)$ to 0 is monotonic. In Fig. 5(b) one sees also that A_σ decreases as $\hbar\omega$ increases.

Finally, we test the accuracy of the single-surface-mode approximation by calculating the energy-loss probability $\Xi(E)$ for a system of aluminum spheres in vacuum. The local dielectric function for the aluminum was modeled by a Drude dielectric function $\epsilon_1(\omega) = 1 - \omega_p^2/(\omega^2 + i\omega/\tau)$, with plasma energy $\hbar\omega_p = 15.8$ eV and two choices of the damping factor $\gamma = 1/\omega_p\tau = 0.01$ and 0.08 . The value $\gamma \approx 0.04$, corresponding to bulk aluminum, lies between the two chosen values. In Fig. 6 we compare an exact calculation of $\Xi(E)$ with the one done using the single surface-mode approximation as defined in Eq. (39). In Fig. 6(a) we plot the energy-loss probability $\Xi(E)$ as a function of the energy loss $E = \hbar\omega$, for spheres of radius $a = 100$ Å, a filling fraction

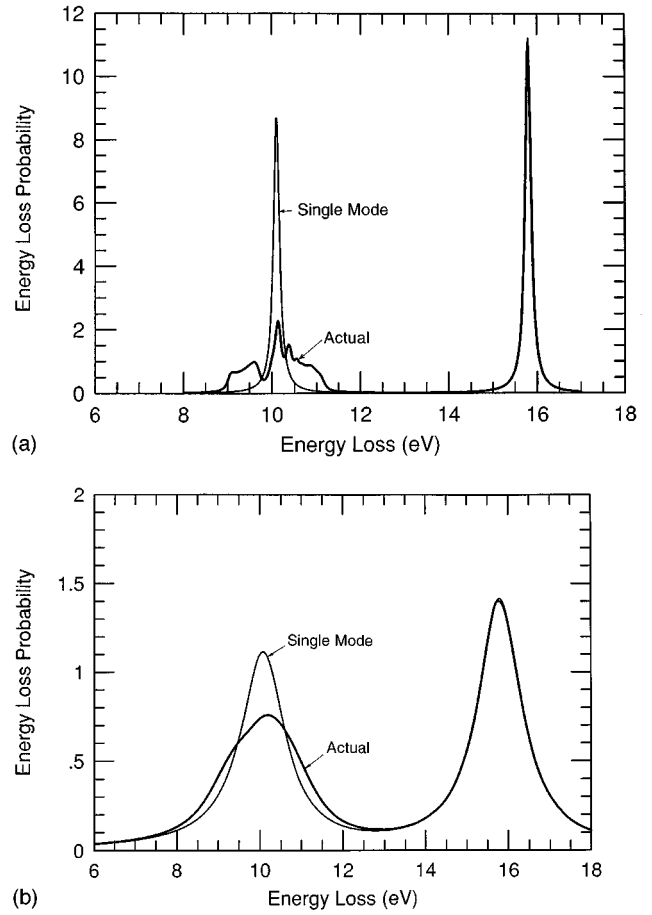


FIG. 6. (a) Energy loss probability density $\Xi(E)$ as a function of the energy loss $E = \hbar\omega$, for a random system of aluminum spheres in vacuum. The spheres have radius $a = 100$ Å, the upper wave vector cutoff is $k_c = 1.69 \text{ \AA}^{-1}$, the incident energy is $E_I = 100$ keV, the filling fractions is $f_1 = 0.1$, and the damping factor γ in the dielectric function of the spheres is $\gamma = 0.01$. The label “Actual” refers to the exact calculation while the label “Single Mode” refers to the calculation in the single-surface-mode approximation. (b) The same as in (a) but with $\gamma = 0.08$.

$f_1 = 0.1$, and a damping factor $\gamma = 0.01$. Such a small damping factor was chosen in order to see the actual structure of the spectral function corresponding to the interfacial modes. One can clearly see that in the single-surface-mode approximation, the actual structure of the interfacial spectral function is replaced by a single mode whose position is located at the centroid of the actual structure. For a larger value of γ the actual surface-mode spectrum will be smoothed out, making the single-surface-mode approximation more accurate. In Fig. 5(b) we show a plot of the energy-loss probability $\Xi(E)$ as a function of the energy loss, for the same parameters as in Fig. 5(a), but with the damping factor γ increased to $\gamma = 0.08$. In this case the single-surface-mode approximation gives a good approximation to the actual spectrum.

In order to facilitate the actual use of the the single-surface-mode approximation we provide, in Appendix C, analytical fits for the bulk strength A_{b_1} and the position of the single effective surface mode α_σ .

IV. COMPARISON WITH THE TRAJECTORY MODEL

Howie and Walsh⁶ have analyzed their experimental data on a system of aluminum inclusions embedded in AlF_3 by calculating the electron energy loss using a model based on a weighted average of electron trajectories. Through the use of phenomenological reasoning and after performing an average over different parts of a typical electron trajectory, they concluded that the local dielectric response $\varepsilon_{\text{HW}}(\omega)$ of an effective medium which could simulate a system of spherical inclusions embedded in an otherwise homogeneous matrix, should be written [see Eq. (5) of Ref. 6] as

$$\frac{1}{\varepsilon_{\text{HW}}} = f_1 \left[\frac{1}{\varepsilon_1} + g_{\text{int}} \left(\frac{3}{\varepsilon_1 + 2\varepsilon_2} - \frac{1}{\varepsilon_1} \right) \right] + f_2 \left[\frac{1}{\varepsilon_2} + g_{\text{ext}} \left(\frac{3}{\varepsilon_1 + 2\varepsilon_2} - \frac{1}{\varepsilon_2} \right) \right], \quad (43)$$

where g_{int} represents the relative importance of interface to bulk excitations in the spheres of material 1, and g_{ext} represents the volume fraction of material 2 which is close enough to a piece of material 1 to give rise to an interface excitation. Here the explicit dependence on ω has been omitted.

Howie and Walsh⁶ argued that for spheres of radius much less than v_I/ω , one should expect $g_{\text{int}} = 1$, which means that the strength of the bulk plasmon in the spheres vanishes. For spheres of larger radius they expected g_{int} to be proportional to $v_I a/\omega$, and so they proposed g_{int} to be independent of f_1 and to be given by a simple expression,

$$g_{\text{int}} = \frac{1}{1 + 3\omega a/v_I}, \quad (44)$$

consistent with these ideas and with numerical results quoted by Echenique *et al.*¹² They also proposed that for small spheres a reasonable dependence of g_{ext} on f_1 should be of the form

$$g_{\text{ext}} = \frac{2f_1}{1 + 2f_1}, \quad (45)$$

at least for small values of f_1 .

It is interesting that Eq. (43) has exactly the same structure as the expression for $\varepsilon_{\text{eff}}(\omega)$ within the single-surface-mode approximation, as given by Eq. (39). In fact, both expressions become identical if one has the following relations between the parameters g_{int} and g_{ext} and the effective strengths A_{b_1} , A_{b_2} , and α_σ :

$$A_{b_1} = f_1(1 - g_{\text{int}}), \quad (46)$$

$$A_{b_2} = f_2(1 - g_{\text{ext}}), \quad (47)$$

and

$$\alpha_\sigma = \frac{1}{3}. \quad (48)$$

Since $A_\sigma = 1 - (A_{b_1} + A_{b_2})$, one has

$$A_\sigma = f_1 g_{\text{int}} + f_2 g_{\text{ext}}. \quad (49)$$

In order to test the validity of Eq. (43) we substitute the values of g_{int} and g_{ext} given by Eqs. (44) and (45) into Eqs. (46) and (47) to yield

$$A_{b_1}^{\text{HW}} = f_1 \frac{3\omega a/v_I}{1 + 3\omega a/v_I} \quad (50)$$

and

$$A_{b_2}^{\text{HW}} = \frac{1 - f_1}{1 + 2f_1}, \quad (51)$$

where the superscript ‘‘HW’’ refers to Howie and Walsh.⁶

In Fig. 1 we compare the dependence of $A_{b_1}^{\text{HW}}/f_1$ on a and $\hbar\omega$, given by Eq. (50), with our expression for A_{b_1}/f_1 , given by Eq. (28), for the same set of external parameters. One can see in Fig. 1(a) that for $\hbar\omega = 16$ eV, $A_{b_1}^{\text{HW}}(a)/f_1$ coincides with $A_{b_1}(a)/f_1$ for $a \approx 20$ Å. For larger values of a , $A_{b_1}^{\text{HW}}(a)/f_1$ is actually larger than $A_{b_1}(a)/f_1$, although it is still a good approximation because the maximum deviation of $A_{b_1}^{\text{HW}}(a)/f_1$ from the exact result is only about 10%. On the other hand, when the sphere radius is fixed at $a = 100$ Å, Fig. 1(b) shows that $A_{b_1}^{\text{HW}}(\omega)/f_1$ deviates substantially from $A_{b_1}(\omega)/f_1$ for $\hbar\omega \leq 5$ eV, but for larger energy losses the deviation is less than about 10%. Therefore $A_{b_1}^{\text{HW}}$ is a reasonable approximation for A_{b_1} . The proposed values of $\alpha_\sigma = 1/3$ and $A_{b_2}^{\text{HW}} = (1 - f_1)/(1 + 2f_1)$ correspond precisely to the $a \rightarrow 0$ limit of α_σ and A_{b_2} , as discussed above. However, the sum rule given in Eq. (41) is satisfied only if $a \approx 0$ and $f_1 \approx 0$, since the value $\alpha_\sigma = 1/3$ is correct only in this limit.

Therefore, one can conclude that the expression proposed by Howie and Walsh [Eq. (43)], for the dielectric response of an effective medium, has exactly the same structure as the spectral representation of $\varepsilon_{\text{eff}}(\omega)$ derived here in the single-surface-mode approximation. However, their expressions for g_{ext} and α_σ become approximately valid only in the $a \rightarrow 0$ and $f_1 \rightarrow 0$ limits. Nevertheless, the theory of Howie and Walsh⁶ might be useful for giving some insight into the physical interpretation of our present theory.

V. SUMMARY

For homogeneous materials, the electron energy-loss spectra of fast electrons can be calculated from the loss function $\text{Im}[-\varepsilon^{-1}(k, \omega)]$; a similar theory⁸ has been found to be very useful for calculating the energy-loss spectra of electrons passing through composite systems consisting of a mixture of two components with local dielectric functions $\varepsilon_1(\omega)$ and $\varepsilon_2(\omega)$. In this theory the macroscopic (or effective) inverse longitudinal dielectric function $\varepsilon_M^{-1}(k, \omega)$ can be written as a spectral representation that contains information about the strengths and positions of bulk longitudinal modes and interfacial modes, which are the excitations responsible for the energy loss.

Here we have derived a spectral representation for $\varepsilon_M^{-1}(k, \omega)$ in which the two components appear on an equal footing. In order to provide a more direct connection between the theory and experiment, an effective local dielectric

function $\varepsilon_{\text{eff}}(\omega)$ has been defined so as to give the same loss spectrum as that calculated from the actual nonlocal dielectric function.

It was also shown that a spectral representation for $1/\varepsilon_{\text{eff}}(\omega)$ also exists and new sum rules that relate the strengths and positions of the modes were also found. In contrast with the usual spectral representation, where the mode strengths and positions depend only on the geometrical structure of the composite, they now depend on both the structure and experimental parameters such as the amount of energy loss, the energy of the incident electrons, and the aperture sizes of the detector. Also, the interfacial modes are not discrete, but form a continuous spectrum.

A useful simplification of the theory is to replace the entire continuum of interfacial modes by a single discrete mode, whose strength and position are the same as the total strength and centroid of all interfacial modes. This single-mode theory contains only four parameters: the strength of the bulk modes of the two components and the strength and position of the single discrete interfacial mode. We calculated these four parameters using our previously developed model of a random system of identical spherical particles, and show how the single-mode theory could be used, with very little effort, to analyze data in which the interfacial modes form a single unresolved energy-loss peak.

The paper ends with a comparison of our single-mode theory with a phenomenological theory developed by Howie and Walsh,⁶ for a random system of spheres. In their theory the structure of the effective local dielectric function is similar to our single-mode theory, but the values proposed for the four parameters were obtained using arguments based on a classical trajectory model. We showed that in their theory, the value proposed for the strength of the bulk mode of the spheres is approximately correct, but the value proposed for the other parameters is applicable only in the limit in which the sizes and volume fraction of the spheres are vanishingly small.

ACKNOWLEDGMENTS

We are pleased to acknowledge very illuminating discussions with A. Howie which stimulated the initial stages of this work. Two of us (R.G.B. and J.L.C.) wish to thank UNESCO and Iowa State University for hospitality at the International Institute of Theoretical and Applied Physics (Ames, Iowa) where part of this work was done. One of us (R.G.B.) acknowledges the financial support of Dirección General de Asuntos del Personal Académico of Universidad Nacional Autónoma de México through Grant Nos. IN-102493 and IN-104195. J.L.C. acknowledges partial financial support by CONACyT (Mexico) Grant No. 2064-E9302. Ames Laboratory is operated for the U.S. Department of Energy by Iowa State University under Contract No. W-7405-Eng-82.

APPENDIX A: EXPRESSIONS FOR C_b , C_s , AND n_s

In this appendix we write down the expressions derived in Ref. 8 for the strengths and location of the bulk and interface modes used in the spectral representation of $\varepsilon_M^{-1}(k, \omega)$ given by Eq. (5), with $\rho^{(2)}(R_{12})$ given by Eq. (7).

The strength of the bulk mode is

$$C_b = 1 - 3 \sum_{l=1}^{\infty} l(2l+1) [j_l(ka)/ka]^2. \quad (\text{A1})$$

The depolarization factors n_s are given by the eigenvalues of a real symmetric matrix

$$H_{ll'} = \frac{1}{2l+1} \delta_{ll'} + 3f \sqrt{l'l'/(2l+1)(2l'+1)} \frac{(l+l')!}{l!(l')!} \times \left(\frac{1}{2}\right)^{l+l'-2} \frac{j_{l+l'-1}(2ka)}{ka}, \quad (\text{A2})$$

and the strengths of the interfacial modes are

$$C_s = 3 \sum_{ll'} \sqrt{l'l'(2l+1)(2l'+1)} \frac{j_l(ka)j_{l'}(ka)}{(ka)^2} U_{ls}U_{l's}, \quad (\text{A3})$$

where j_l is the spherical Bessel function of order l , and U_{ls} is the unitary matrix which diagonalizes $H_{ll'}$, that is,

$$\sum_{ll'} U_{sl}^{-1} H_{ll'} U_{l's'} = n_s \delta_{ss'}. \quad (\text{A4})$$

APPENDIX B: DISCRETE APPROXIMATION

Although the discrete surface-mode parameters A_s , α_s , A_{σ} , and α_{σ} , are defined by Eqs. (32), (33), (23), (37), and (38), these equations are not actually useful for calculating these quantities, as we discussed in the text. A useful expression for the mode strength A_s is found omitting the denominators $n_s \varepsilon_1 + (1 - n_s) \varepsilon_2$ from the left-hand side of Eq. (21) and making the same change of variable of integration from k to n . This procedure gives

$$W \int_{\omega/v_1}^{k_c} G_s(k) \frac{dk}{k} = \int_0^1 \mathcal{A}_s(n) dn, \quad (\text{B1})$$

and using the definition of A_s in Eq. (32), we have

$$A_s = W \int_{\omega/v_1}^{k_c} G_s(k) \frac{dk}{k}. \quad (\text{B2})$$

This result is identical to Eq. (20), except that the index j in Eq. (20) can now run over interfacial modes s in addition to the bulk modes b_1 and b_2 .

The total strength of all surface modes is

$$A_{\sigma} = \sum_s A_s = W \int_{\omega/v_1}^{k_c} \sum_s G_s(k) \frac{dk}{k}. \quad (\text{B3})$$

Similarly, an expression for $\alpha_s A_s$ is found from the equation

$$\begin{aligned}\alpha_s A_s &= \int n \mathcal{A}_s(n) dn \\ &= W \int_{\omega/v_I}^{k_c} n_s(k) G_s(k) \frac{dk}{k},\end{aligned}\quad (\text{B4})$$

which is derived using the same change of variable as in Eqs. (21) and (22). Summing over s and using Eq. (38), we get

$$\alpha_\sigma A_\sigma = W \int_{\omega/v_I}^{k_c} \sum_s n_s(k) G_s(k) \frac{dk}{k}. \quad (\text{B5})$$

From Eqs. (B3) and (B5) we have

$$\alpha_\sigma = \int_{\omega/v_I}^{k_c} \sum_s n_s(k) G_s(k) \frac{dk}{k} \bigg/ \int_{\omega/v_I}^{k_c} \sum_s G_s(k) \frac{dk}{k}. \quad (\text{B6})$$

Equation (B6) reduces to Eq. (42) after making the substitution $G_s = f_1 C_s / n_s$ and changing the integration variable from k to $x = ka$.

APPENDIX C: PRACTICAL FORMULAS

In this appendix we provide analytical expressions for A_{b_1} and α_σ , k_I , and $\omega a/v_I$. For A_{b_1} we get

$$A_{b_1} = f_1 W \ln \left[\frac{b + \sqrt{(k_c a)^2 + b^2}}{b + \sqrt{\zeta^2 + b^2}} \right], \quad (\text{C1})$$

where

$$b = 2.3471,$$

$$\zeta = \omega a/v_I,$$

$$W = 1/\ln(k_c v_I/\omega). \quad (\text{C2})$$

For α_σ we get,

$$\alpha_\sigma = S(\zeta) + H(f_1) T(\zeta), \quad (\text{C3})$$

where

$$\begin{aligned}S(\zeta) &= 0.4531 - 0.04669\zeta + 0.030282\zeta^2 - 6.604 \times 10^{-3}\zeta^3 \\ &\quad + 6.0 \times 10^{-4}\zeta^4 - 1.81 \times 10^{-5}\zeta^5 \quad (\zeta \leq 6)\end{aligned}\quad (\text{C4})$$

$$\begin{aligned}T(\zeta) &= 1/(0.271 + 0.194\zeta^{1.08}) - 1.14 \quad (\zeta < 1.66) \\ &= 1.585\zeta^{-2.24} \quad (\zeta \geq 1.66)\end{aligned}\quad (\text{C5})$$

and

$$H(f_1) = 0.18272(f_1 - 0.2) - 0.0643(f_1 - 0.2)^2. \quad (\text{C6})$$

Equations (C1)–(C6) fit the exact calculations with an error of less than 1%.

The wave vector k_I for an incident electron with kinetic energy E_I is

$$k_I = (0.512 \text{ \AA}^{-1}) \sqrt{1 + x/2} \sqrt{E_I}, \quad (\text{C7})$$

where

$$x = E_I/m_e c^2 = 1.957 \times 10^{-6} E_I. \quad (\text{C8})$$

For a typical energy $E_I = 100$ keV we find $k_I = 170 \text{ \AA}^{-1}$, giving a cutoff wave vector $k_c \approx k_I \theta \approx 1.7 \text{ \AA}^{-1}$ if the maximum deflection angle in the scanning electron microscopy experiment is $\theta \approx 10$ mrad. For the dimensionless parameter $\zeta = \omega a/v_I$ we have the formula

$$\omega a/v_I = 0.256 R(x) \hbar \omega a / \sqrt{E_I}, \quad (\text{C9})$$

where $R(x) = (1+x)/\sqrt{1+x/2}$ is a relativistic correction. In Eqs. (C7)–(C9), E_I and $\hbar \omega$ are expressed in eV and a is expressed in \AA.

¹See, for example, R. Landauer, in *Electrical Transport and Optical Properties of Inhomogeneous Media*, edited by J. C. Garland and D. B. Tanner, AIP Conf. Proceedings, Number 40 (AIP, New York, 1978), pp. 2–45.

²J. C. Maxwell Garnett, *Philos. Trans. R. Soc. London* **203**, 385 (1904).

³D. A. G. Bruggeman, *Ann. Phys. (Leipzig)* **24**, 636 (1935).

⁴See, for example, R. G. Barrera, P. Villaseñor-González, W. Luis Mochán, and G. Monsivais, *Phys. Rev. B* **41**, 7370 (1990), and references therein.

⁵C. Walsh, *Philos. Mag. A* **59**, 227 (1989).

⁶A. Howie and C. A. Walsh, *Microsc. Microanal. Microstruct.* **2**, 171 (1991).

⁷J. B. Pendry and L. M. Moreno, *Phys. Rev. B* **50**, 5062 (1994).

⁸R. G. Barrera and R. Fuchs, *Phys. Rev. B* **52**, 3256 (1995).

⁹D. J. Bergman, *Phys. Rep.* **43**, 377 (1978); G. W. Milton, *J. Appl. Phys.* **52**, 5286 (1981); R. Fuchs and F. Claro, *Phys. Rev. B* **46**, 12955 (1992); R. Fuchs, *ibid.* **11**, 1732 (1975).

¹⁰In the $k \rightarrow 0$ limit there is no distinction between the longitudinal response discussed here and the transverse response used to describe propagation of electromagnetic waves.

¹¹This spectral representation should be also valid for any two-component composite of arbitrary geometry.

¹²P. M. Echenique, J. Bausells, and A. Rivacoba, *Phys. Rev. B* **35**, 1521 (1987).